The magnetic structure factor of the square ice: A phenomenological description

N. Rougemaille, Benjamin Canals

The magnetic structure factor of the square ice: A phenomenological description

Cite as: Appl. Phys. Lett. **118**, 112403 (2021); https://doi.org/10.1063/5.0043520
Submitted: 08 January 2021 . Accepted: 27 February 2021 . Published Online: 16 March 2021

N. Rougemaille, and B. Canals

Applied Physics Letters ARTICLE scitation.org/journal/apl

The magnetic structure factor of the square ice: A phenomenological description

Cite as: Appl. Phys. Lett. **118**, 112403 (2021); doi: 10.1063/5.0043520
Submitted: 8 January 2021 · Accepted: 27 February 2021 ·
Published Online: 16 March 2021

N. Rougemaille[a] and B. Canals

AFFILIATIONS

Université Grenoble Alpes, CNRS, Grenoble INP, Institut NEEL, 38000 Grenoble, France

Note: This paper is part of the APL Special Collection on Mesoscopic Magnetic Systems: From Fundamental Properties to Devices.
[a]**Author to whom correspondence should be addressed:** nicolas.rougemaille@neel.cnrs.fr

ABSTRACT

We consider the sixteen vertex model, and we describe, phenomenologically, the main features of the square ice magnetic structure factor. Using Monte Carlo simulations, we show that in the high-temperature regime, the magnetic structure factor of the square ice can be seen as the superposition of two distinct magnetic structure factors associated with two other models. In particular, we provide empirical arguments to explain why intensity is present in some regions of reciprocal space and absent in other locations. We also tentatively explain why the so-called pinch points, evidencing the algebraic nature of the spin-spin correlations once the system is brought into its ground state manifold, appear for certain wavevectors only.

Lithographically patterned arrays of interacting magnetic nanoislands have received considerable attention over the last decade.[1–3] To a large extent, this attention is due to the capability of these arrays to mimic the exotic many body physics of highly frustrated magnets and to visualize this physics directly, in real space[4–6] and in real time.[7,8] If the initial motivation was to realize an artificial kagome[9–13] and square[12–16] ice magnet, a wide range of artificial systems have been now investigated, including structures that have no counterparts in bulk materials.[17–28]

Although artificial systems can be imaged in real space, the spin ice physics is often better approached in reciprocal space. In particular, the magnetic structure factor (MSF) is a powerful tool to probe pairwise spin correlations in k space. Since the magnetic states of artificial frustrated magnets are directly accessible, the associated MSF can be reconstructed *a posteriori*, i.e., without being measured. The MSF was used, for example, to evidence a fragmentation process in artificial dipolar kagome ices,[29–33] to reveal a Coulomb phase physics in artificial kagome[34] and square ice magnets,[35–37] and to propose a complex magnetic order in the dipolar kagome Ising antiferromagnet.[38–40]

When the ground state is ordered, the MSF is relatively simple to grasp: magnetic Bragg peaks appear for specific wavevectors. However, when the ground state is disordered, in the manner of a spin liquid, the MSF is diffuse, yet structured. In that case, explaining why a magnetic signal is present in some regions of reciprocal space and not in others is not an easy task. The purpose of this work is to describe, *phenomenologically*, the shape of the square ice MSF in the high-temperature limit and to provide an *empirical* understanding of the spin-spin correlations that develop in the ice manifold. Using Monte Carlo simulations, we compute the MSF of several variants of the sixteen vertex model and numerically demonstrate that, *at high temperature*, the square ice MSF results from the superposition of two other magnetic structure factors.

In statistical mechanics, a vertex model is a model in which a statistical weight is attributed to the nodes of a graph, the state of a node being defined by the state of each of its bonds. In this work, we consider a two-dimensional square lattice with bonds that can be only in two possible states, say a state "in" or a state "out" with respect to the vertex center. Each vertex being the merging point of four bonds can be in one of the 2^4 possible states. Such a model is called the sixteen vertex model. The sixteen possible vertex states are represented in Fig. 1(a). As we consider a spin system, the state of a given bond is nothing else than a spin direction. Assuming time reversal symmetry, the sixteen vertices can be sorted in four different groups [see the four colors in Figs. 1(a) and 1(b)].

The spin Hamiltonian used in this work to investigate the properties of the sixteen vertex model can be written as

$$\mathcal{H} = -J_1 \sum_{\langle ij \rangle} \sigma_i \sigma_j - J_2 \sum_{\langle\langle ij \rangle\rangle} \sigma_i \sigma_j, \quad (1)$$

where σ_i and σ_j are the Ising variables on the sites i and j, whereas J_1 and J_2 are the coupling strengths between perpendicular and collinear

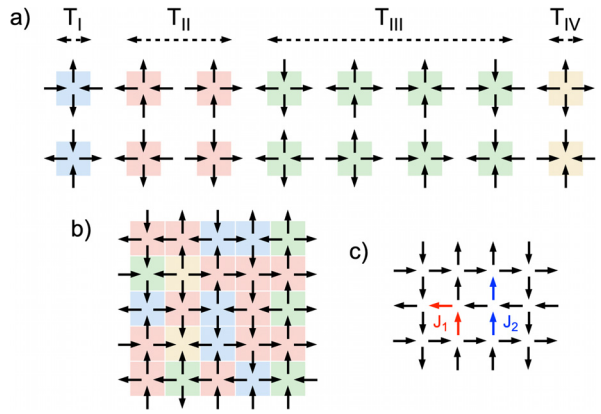

FIG. 1. (a) Schematics of all possible vertices in the sixteen vertex model. The vertices can be sorted in four groups according to their symmetry: type I (blue, T_I), type II (red, T_{II}), type III (green, T_{III}), and type IV (yellow, T_{IV}) vertices. (b) Example of a spin configuration involving all four vertex types. (c) Schematics of the coupling strengths in the associated spin model, in which two coupling constants can be defined: J_1, between nearest neighbors belonging to the two sublattices of the square lattice (perpendicular spins, in red), and J_2, between nearest neighbors belonging to the same sublattice (collinear spins, in blue).

nearest neighbors, respectively [no further neighbor interactions are considered [see Fig. 1(c)]. Both coupling strengths have positive values, thus favoring ferromagnetic interactions.

In the following, we consider three cases depending on the value of the $\alpha = J_1/J_2$ ratio:

- $\alpha > 1$, when the blue (T_I) vertices have a higher statistical weight than the red ones (T_{II} vertices). The ground state is then antiferromagnetically ordered and two times degenerate [see Fig. 2(a) for one possible configuration].
- $\alpha < 1$, when the condition is the opposite. The ground state is (sub)extensively degenerate and made of decoupled ferromagnetic lines crossing the entire lattice [see Fig. 2(b) for one possible configuration].
- The square ice is the peculiar case when all six T_I and T_{II} vertices have the same statistical weight,[41] i.e., when $\alpha = 1$. The ground state is macroscopically degenerate. Although disordered [see Fig. 2(c) for one possible configuration], the phase is correlated and pairwise spin correlations decay algebraically with the separation distance.[35]

The ground state magnetic structure factors of these three models are reported in Figs. 2(d)–2(f). With the ground state of the $\alpha > 1$ model being antiferromagnetically ordered [see Fig. 2(a)], the MSF is characterized by magnetic Bragg peaks at the corners of the Brillouin zone. The ground state manifold of the $\alpha < 1$ model consists of

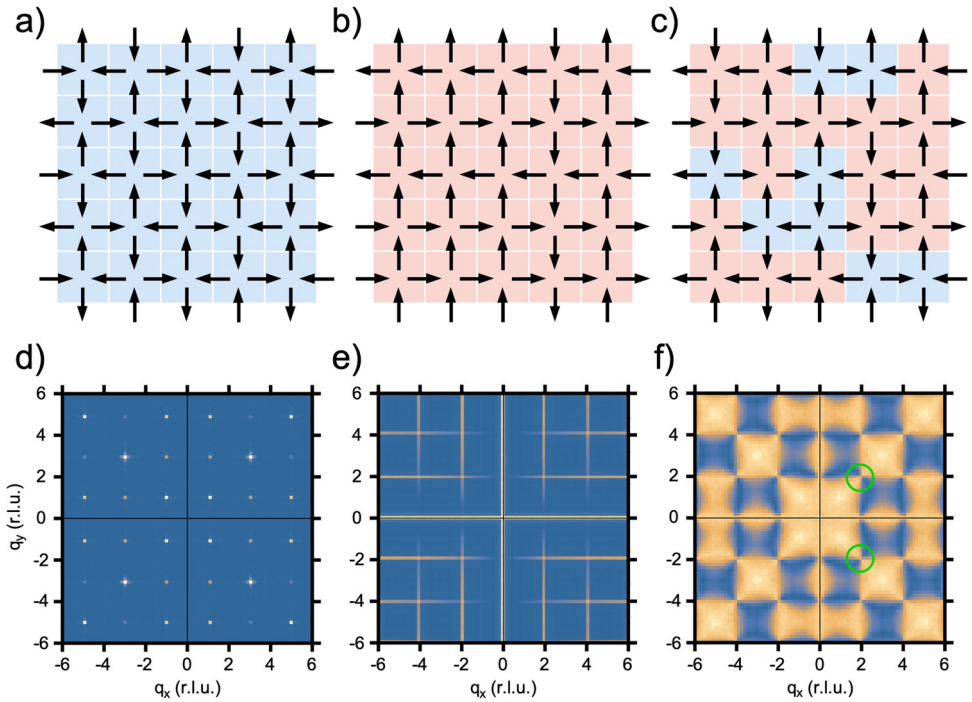

FIG. 2. Real space (a)–(c) and reciprocal space (d)–(f) representation of the ground state manifold of the $\alpha > 1$ (a) and (d), $\alpha < 1$ (b) and (e) and square ice ($\alpha = 1$) models (c) and (f). The ground state of the $\alpha > 1$ model is antiferromagnetic and two times degenerate: it consists of a tiling of T_I (blue) vertices (a) and Bragg peaks in the corners of the Brillouin zone (d). The ground state of the $\alpha < 1$ model is made of a random arrangement of fully polarized lines (T_{II} vertices) spanning across the lattice (b) and, thus, lines in reciprocal space (e). The $\alpha < 1$ manifold is extensively degenerate, although the degeneracy is subextensive. The square ice $\alpha = 1$ is a paramagnet of T_I and T_{II} vertices (c), characterized by a diffuse, yet structured, magnetic structure factor (f). The square ice manifold is macroscopically degenerate. The green circle in (f) indicates the locations of singularities, the so-called pinch points.

random arrangements of fully polarized lines [see Fig. 2(b)], and the associated MSF exhibits well-defined lines. Note that magnetic Bragg peaks are absent in this MSF as there is no long range order: the manifold is made of a (sub)extensive number of configurations, i.e., the residual entropy tends to zero as the system approaches the thermodynamic limit. The MSF of the square ice consists of a diffuse, yet structured, background signal. This MSF is typical of a cooperative paramagnet, i.e., a highly disordered, correlated spin manifold. The algebraic nature of the spin-spin correlations in real space translates into singularities in reciprocal space, the so-called pinch points[42–45] [see green circles in Fig. 2(f)].

We now investigate the high-temperature regime of the three models. To do so, we performed Monte Carlo simulations based on the spin Hamiltonian shown in Eq. (1). The simulations were performed for $12 \times 12 \times 2$ lattice sites, with periodic boundary conditions. A single spin flip algorithm was used as we are only interested in the high-temperature regime in which the acceptation rate of the spin dynamics remains large. Following previous works,[46] the cooling procedure starts from $T/J = 100$ and 10^4 Monte Carlo steps are used for thermalization. Measurements follow the thermalization and are also computed with 10^4 Monte Carlo steps.

The temperature dependence of the magnetic structure factors are represented in Fig. 3 for different temperatures expressed in J units [$J = \max(J_1, J_2)$]. As expected, the $\alpha > 1$ model leads to emergent magnetic Bragg peaks as the temperature is reduced [see Fig. 3(a)], and at $T/J = 6.9$, they are all clearly visible. One of these Bragg peaks is highlighted by a red circle in Fig. 3(a). Because the temperature is high, the Bragg peaks are very broad and weakly intense as compared

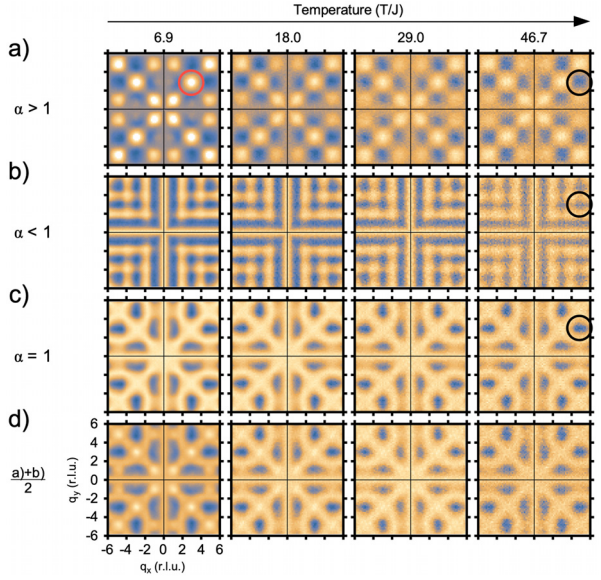

FIG. 3. Temperature dependence of the magnetic structure factors of the $\alpha > 1$ (a), $\alpha < 1$ (b), and $\alpha = 1$ (c) models. The temperature, normalized to the nearest-neighbor coupling strength $J = \max(J_1, J_2)$, is indicated. (d) The comparison between the $\alpha = 1$ model and the average of the $\alpha > 1$ and $\alpha < 1$ models is striking. The red and black circles highlight specific locations in reciprocal space that are discussed in the text.

to those observed in the ground state [see Fig. 2(d)]. As also expected, the magnetic structure factor of the $\alpha < 1$ model is characterized by emerging lines in specific directions, for example, along the $q_x = 0$ and $q_y = 0$ directions [see black lines in Fig. 3(b)]. Similar to the $\alpha > 1$ case, the features observed in reciprocal space remain very broad compared to those of the ground state [see Fig. 2(e)] since the temperature is high. In the case of the square ice model, the MSF is extremely diffuse as the system remains strongly disordered [see Fig. 3(c)] in the temperature range we probe here. However, although the temperature is high, the main features of the MSF expected in the low-energy manifold [see Fig. 2(f)] are already visible, indicating that the spin-spin correlations start to develop. Overall, despite the fact that the thermal energy (k_B T, with the Boltzmann constant set to 1) is substantially larger than the coupling strengths, the MSFs of these three variants of the sixteen vertex model are clearly distinct and are already reminiscent of the ground state MSFs reported in Fig. 2.

It is interesting to note that the intensity of the MSF in the $\alpha > 1$ and $\alpha < 1$ models increases in distinct regions of reciprocal space. This can be seen, for example, by looking at the MSF for the lowest temperatures: the emergent Bragg peaks in Fig. 3(a) pop up precisely where the signal vanishes in Fig. 3(b). Similarly, the intensity of the lines appearing in the MSF of the $\alpha < 1$ model increases where it goes away in the MSF of the $\alpha > 1$ model. This shows that the associated spin-spin correlations have distinct signatures in reciprocal space, as one would expect from the MSF ground state [see Figs. 2(d) and 2(e)]. Nevertheless, some regions of the (q_x, q_y) plane are quickly depleted in both MSFs [see the black circles in Figs. 3(a) and 3(b) at the highest temperatures], suggesting that specific spin-spin correlations are removed in the two models [and, in fact, in the square ice model as well [see Fig. 3(c)].

Taken as a whole, these observations can be explained phenomenologically by recalling that the sixteen vertex model is described by four vertex energies [see Fig. 1(a)]. At infinite temperature, all vertex types are populated according to their degeneracy. Whatever the considered model, the system is then an ideal paramagnet; all pairwise spin correlations are zero on average, and the MSF is flat. As the temperature is reduced, the energy hierarchy between the vertex types starts to be probed. The population of T_{IV} vertices [the yellow vertices in Fig. 1(a)] is reduced first.[47] We then argue that the regions where the intensity drops at the highest temperatures [within the black circles in Figs. 3(a)–3(c)] correspond to the spin correlations associated with the presence of T_{IV} vertices (this point will be confirmed below).

Since the $\alpha > 1$ model favors the formation of T_I vertices, whereas the $\alpha < 1$ model favors the formation of T_{II} vertices, we might wonder whether the square ice, which is a random arrangement of both vertex types, develops spin correlations that can be deduced from these two models. To test this idea, we averaged the MSF of the two models and compared it with the one of the square ice for different temperatures. Surprisingly, there is no visible difference at high temperature, and the averaged MSF [see Fig. 3(d)] is hardly distinguishable from the one of the square ice [see Fig. 3(c)]. The striking observation here is that the signal constituting the emergent Bragg peaks in Fig. 3(a) complements very nicely the vanishing signal in Fig. 3(b), at least in a certain temperature range. As the temperature is further reduced, the intensity within the Bragg peaks quickly increases, and the peaks become narrower as the system further correlates. At a normalized temperature of about 18, the two MSFs do not

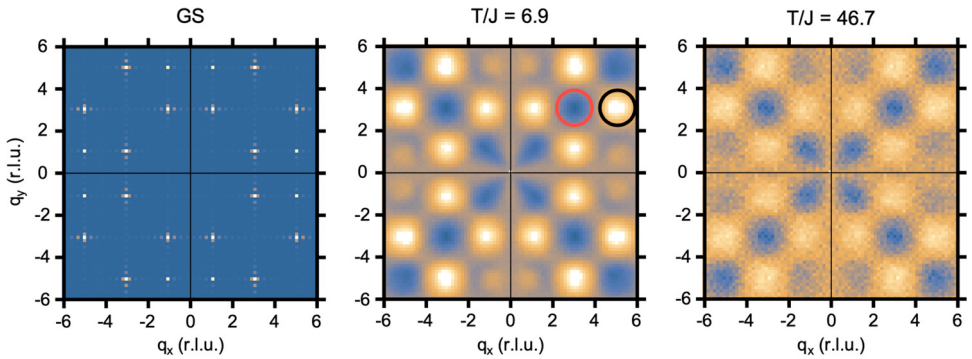

FIG. 4. Temperature dependence of the MSF of the "all-in/all-out" model: $J_1 = -1$, $J_2 = 0$. Three (normalized) temperatures are shown: the lowest accessible one corresponding to the ground state (GS), 6.9 and 46.7.

complement themselves perfectly and deviations with the square ice MSF are observed.

In a certain temperature range, the pairwise spin correlations of the square ice must be similar to those of the $\alpha > 1$ and $\alpha < 1$ models combined. This result is not intuitive. In the high-temperature regime we study, all three manifolds essentially consist of a mixture of T_I, T_{II}, and T_{III} vertices (we can neglect the contribution of T_{IV} vertices (see Ref. 47). From this argument alone, one would expect a similar MSF for the three models. But this is clearly not what we observe, indicating that distinct spin-spin correlations develop in all three cases. However, the spin correlations that vanish in one of the two models are strengthened in the other one in such a way that adding them together provides those of the high-temperature ice manifold.

As mentioned above, all three models have a high-temperature MSF exhibiting negligible spin correlations in specific regions of reciprocal space [see black circles in Figs. 3(a)–3(c)]. To demonstrate that these regions correspond to spin correlations associated with the presence of T_{IV} vertices, we computed the thermodynamic properties of the same spin Hamiltonian [see Eq. (1)] with $J_1 < 0$ (antiferromagnetic coupling) and $J_2 = 0$. An "all-in/all-out" ground state (i.e., a tiling of T_{IV} vertices only) is then favored [see Fig. 4]. The corresponding Bragg peaks are precisely located in the regions where

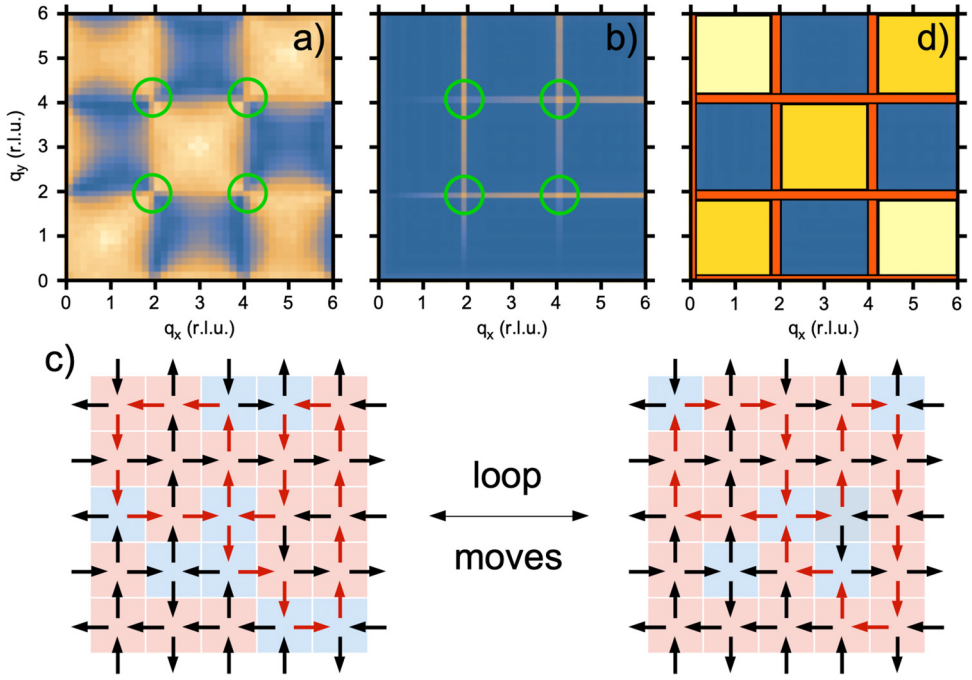

FIG. 5. [(a) and (b)] Magnetic structure factor of the ice and $\alpha < 1$ models for (q_x, q_y) values ranging from 0 to 6 reciprocal lattice units (r.l.u.). The regions where pinch points are observed in (a) are highlighted by green circles. The corresponding regions in (b) are also marked by green circles. Pinch points in (a) correspond to locations where lines intersect in (b). (c) Schematics of the loop dynamics involved at low temperature. Two loop moves are represented in red, allowing us to explore the ice manifold while preserving the divergence-free constraint. (d) Schematics of the square ice MSF. The red bars correspond to the intensity originating from the $\alpha < 1$ model, whereas the yellow and orange squares correspond to the signal induced in the $\alpha > 1$ model. The orange/yellow colors are used to indicate a higher/lower intensity.

the intensity vanishes in the three models [see black circles in Figs. 3(a), 3(b), and 3(c)]. This confirms that T_{IV} vertices play a minor role in the high-temperature limit.

At this point, we note that the results presented in Fig. 3 depend on the values of the J_1 and J_2 coupling strengths used in the Monte Carlo simulations. In particular, the $\alpha > 1$ and $\alpha < 1$ models require different values for these two coupling strengths. One could choose them in such a way that one equals 1 and the other 0 (as we did here), but one could also choose much closer values (1 and 0.5, for example). For nearly identical values, we expect to find an ice-like regime down to low temperatures, regardless of the model ($\alpha > 1$ or $\alpha < 1$). As these values are detuned, we expect the transition to the ground state to occur at a higher critical temperature. In fact, the $\alpha = J_1/J_2$ ratio is an external parameter that we can play with to adjust the temperature at which the transition occurs.[46] Consequently, the temperature range for which a good match is observed between the high-temperature ice manifold and the one resulting from the average of the $\alpha > 1$ and $\alpha < 1$ models depends on the α value. However, whatever the J_1 and J_2 values, there always exists a temperature range for which the MSFs are hardly distinguishable.

It is also worth mentioning that the pinch points observed in the ground state manifold of the square ice [see green circles in Fig. 5(a)] appear for wavevectors where lines intersect in the magnetic structure factor of the $\alpha < 1$ model [see Fig. 5(b)]. For these peculiar wavevectors, there is no signal in the ground state MSF of the $\alpha > 1$ model [see Fig. 2(d)]. Although the points where lines intersect in Fig. 5(b) are not singularities, an intensity scan through such a point may vary abruptly depending on how the intersect is approached. In that sense, they share some properties of the pinch points. We then speculate that the spin correlations associated with the pinch points in the square ice correspond to correlations within magnetic lines. But contrary to the $\alpha < 1$ model, these lines do not (necessarily) cross the entire lattice along one direction, but rather form closed loops (because the ice manifold is a mixture of T_I and T_{II} vertices). Within the ice manifold, we indeed know that spin loops, such as those highlighted in red in Fig. 5(c), are the only possible spin updates to jump from one ice configuration to another. It is then tempting to argue that the presence of pinch points, and thus, the presence of algebraic pairwise spin correlations in Ising frustrated systems, is intimately linked to a loop/string physics.[48]

Finally, a phenomenological description of the square ice MSF can be drawn from our observations. This MSF can be schematically cut in different sectors that can be attributed to either the $\alpha > 1$ or $\alpha < 1$ models [see Fig. 5(d)]. The spin correlations induced by the $\alpha < 1$ model correspond to the red rectangles in Fig. 5(d), whereas those originating from the $\alpha > 1$ model are represented by yellow/orange squares. It is interesting to note that the intensity slightly varies between sectors. In particular, the intensity is higher (orange) in the (11) direction of the (q_x, q_y) plane than in the other regions (yellow). This asymmetry in the intensity distribution is also found in the $\alpha > 1$ model [see, for example, Fig. 3(a)] at $T/J = 18.0$. In a first approximation, the MSF of the square ice can then be divided into (q_x, q_y) pockets having distinct origins. Our phenomenological description also provides a visual illustration of the origin of the pinch points that characterize ice magnets.

AUTHORS' CONTRIBUTIONS

All the authors contributed equally to this work.

This work was supported by the Agence Nationale de la Recherche through Project No. ANR-17-CE24–0007-03 "Bio-Ice". N.R. warmly thanks V. Schánilec and O. Brunn for careful reading of this manuscript.

DATA AVAILABILITY

The data that support the findings of this study are available from the corresponding author upon reasonable request.

REFERENCES

[1]C. Nisoli, R. Moessner, and P. Schiffer, Rev. Mod. Phys. **85**, 1473 (2013).
[2]N. Rougemaille and B. Canals, Eur. Phys. J. B **92**, 62 (2019).
[3]S. H. Skjærvø, C. H. Marrows, R. L. Stamps, and L. J. Heyderman, Nat. Rev. Phys. **2**, 13 (2020).
[4]M. Tanaka, E. Saitoh, H. Miyajima, T. Yamaoka, and Y. Iye, J. Appl. Phys. **97**, 10J710 (2005).
[5]M. Tanaka, E. Saitoh, H. Miyajima, T. Yamaoka, and Y. Iye, Phys. Rev. B **73**, 052411 (2006).
[6]R. F. Wang, C. Nisoli, R. S. Freitas, J. Li, W. McConville, B. J. Cooley, M. S. Lund, N. Samarth, C. Leighton, V. H. Crespi, and P. Schiffer, Nature **439**, 303 (2006).
[7]A. Farhan, P. M. Derlet, A. Kleibert, A. Balan, R. V. Chopdekar, M. Wyss, J. Perron, A. Scholl, F. Nolting, and L. J. Heyderman, Phys. Rev. Lett. **111**, 057204 (2013).
[8]A. Farhan, A. Kleibert, P. M. Derlet, L. Anghinolfi, A. Balan, R. V. Chopdekar, M. Wyss, S. Gliga, F. Nolting, and L. J. Heyderman, Phys. Rev. B **89**, 214405 (2014).
[9]Y. Qi, T. Brintlinger, and J. Cumings, Phys. Rev. B **77**, 094418 (2008).
[10]S. Ladak, D. E. Read, G. K. Perkins, L. F. Cohen, and W. R. Branford, Nat. Phys. **6**, 359 (2010).
[11]E. Mengotti, L. J. Heyderman, A. Fraile Rodríguez, F. Nolting, R. V. Hügli, and H.-B. Braun, Nat. Phys. **7**, 68 (2011).
[12]J. Li, X. Ke, S. Zhang, D. Garand, C. Nisoli, P. Lammert, V. H. Crespi, and P. Schiffer, Phys. Rev. B **81**, 092406 (2010).
[13]C. Nisoli, J. Li, X. Ke, D. Garand, P. Schiffer, and V. H. Crespi, Phys. Rev. Lett. **105**, 047205 (2010).
[14]J. P. Morgan, A. Stein, S. Langridge, and C. H. Marrows, Nat. Phys. **7**, 75 (2011).
[15]J. P. Morgan, A. Stein, S. Langridge, and C. H. Marrows, New J. Phys. **13**, 105002 (2011).
[16]V. Kapaklis, U. B. Arnalds, A. Harman-Clarke, E. Th. Papaioannou, M. Karimipour, P. Korelis, A. Taroni, P. C. W. Holdsworth, S. T. Bramwell, and B. Hjörvarsson, New J. Phys. **14**, 035009 (2012).
[17]I. Gilbert, G.-W. Chern, S. Zhang, L. O'Brien, B. Fore, C. Nisoli, and P. Schiffer, Nat. Phys. **10**, 670 (2014).
[18]H. Stopfel, E. Östman, I.-A. Chioar, D. Greving, U. B. Arnalds, T. P. A. Hase, A. Stein, B. Hjörvarsson, and V. Kapaklis, Phys. Rev. B **98**, 014435 (2018).
[19]I. Gilbert, Y. Lao, I. Carrasquillo, L. O'Brien, J. D. Watts, M. Manno, C. Leighton, A. Scholl, C. Nisoli, and P. Schiffer, Nat. Phys. **12**, 162 (2016).
[20]A. Farhan, C. F. Petersen, S. Dhuey, L. Anghinolfi, Q. H. Qin, M. Saccone, S. Velten, C. Wuth, S. Gliga, P. Mellado, M. J. Alava, A. Scholl, and S. van Dijken, Nat. Commun. **8**, 995 (2017).
[21]V.-D. Nguyen, Y. Perrin, S. L. Denmat, B. Canals, and N. Rougemaille, Phys. Rev. B **96**, 014402 (2017).
[22]E. Östman, U. B. Arnalds, V. Kapaklis, A. Taroni, and B. Hjörvarsson, J. Phys.: Condens. Matter **30**, 365301 (2018).
[23]I. R. B. Ribeiro, F. S. Nascimento, S. O. Ferreira, W. A. Moura-Melo, C. A. R. Costa, J. Borme, P. P. Freitas, G. M. Wysin, C. I. L. de Araujo, and A. R. Pereira, Sci. Rep. **7**, 13982 (2017).
[24]R. P. Loreto, F. S. Nascimento, R. S. Gonçalves, J. Borme, J. C. Cezar, C. Nisoli, A. R. Pereira, and C. I. L. de Araujo, J. Phys.: Condens. Matter **31**, 025301 (2019).
[25]G. M. Macauley, G. W. Paterson, Y. Li, R. Macêdo, S. McVitie, and R. L. Stamps, Phys. Rev. B **101**, 144403 (2020).

[26]M. Massouras, D. Lacour, M. Hehn, and F. Montaigne, Phys. Rev. B **101**, 174421 (2020).
[27]D. Shi, Z. Budrikis, A. Stein, S. A. Morley, P. D. Olmsted, G. Burnell, and C. H. Marrows, Nat. Phys. **14**, 309 (2018).
[28]F. Barrows, V. Brajuskovic, A. K. Petford-Long, and C. Phatak, Phys. Rev. B **99**, 094424 (2019).
[29]N. Rougemaille, F. Montaigne, B. Canals, A. Duluard, D. Lacour, M. Hehn, R. Belkhou, O. Fruchart, S. E. Moussaoui, A. Bendounan, and F. Maccherozzi, Phys. Rev. Lett. **106**, 057209 (2011).
[30]S. Zhang, I. Gilbert, C. Nisoli, G.-W. Chern, M. J. Erickson, L. OBrien, C. Leighton, P. E. Lammert, V. H. Crespi, and P. Schiffer, Nature **500**, 553 (2013).
[31]I. A. Chioar, B. Canals, D. Lacour, M. Hehn, B. S. Burgos, T. O. Mentes, A. Locatelli, F. Montaigne, and N. Rougemaille, Phys. Rev. B **90**, 220407(R) (2014).
[32]B. Canals, I. A. Chioar, V. D. Nguyen, M. Hehn, D. Lacour, F. Montaigne, A. Locatelli, T. O. Menteş, B. S. Burgos, and N. Rougemaille, Nat. Commun. **7**, 11446 (2016).
[33]V. Schánilec, B. Canals, V. Uhlíř, L. Flajšman, J. Sadílek, T. Šikola, and N. Rougemaille, Phys. Rev. Lett. **125**, 057203 (2020).
[34]O. Sendetskyi, L. Anghinolfi, V. Scagnoli, G. Möller, N. Leo, A. Alberca, J. Kohlbrecher, J. Luning, U. Staub, and L. J. Heyderman, Phys. Rev. B **93**, 224413 (2016).
[35]Y. Perrin, B. Canals, and N. Rougemaille, Nature **540**, 410 (2016).
[36]E. Östman, H. Stopfel, I.-A. Chioar, U. B. Arnalds, A. Stein, V. Kapaklis, and B. Hjörvarsson, Nat. Phys. **14**, 375 (2018).
[37]A. Farhan, M. Saccone, C. F. Petersen, S. Dhuey, R. V. Chopdekar, Y.-L. Huang, N. Kent, Z. Chen, M. J. Alava, T. Lippert, A. Scholl, and S. van Dijken, Sci. Adv. **5**, eaav6380 (2019).
[38]S. Zhang, J. Li, I. Gilbert, J. Bartell, M. J. Erickson, Y. Pan, P. E. Lammert, C. Nisoli, K. K. Kohli, R. Misra, V. H. Crespi, N. Samarth, C. Leighton, and P. Schiffer, Phys. Rev. Lett. **109**, 087201 (2012).
[39]I. A. Chioar, N. Rougemaille, A. Grimm, O. Fruchart, E. Wagner, M. Hehn, D. Lacour, F. Montaigne, and B. Canals, Phys. Rev. B **90**, 064411 (2014).
[40]I. A. Chioar, N. Rougemaille, and B. Canals, Phys. Rev. B **93**, 214410 (2016).
[41]E. H. Lieb, Phys. Rev. **162**, 162 (1967).
[42]M. P. Zinkin and M. J. Harris, J. Magn. Magn. Mater. **140-144**, 1803 (1995).
[43]C. L. Henley, Phys. Rev. B **71**, 014424 (2005).
[44]C. L. Henley, Annu. Rev. Condens. Matter Phys. **1**, 179 (2010).
[45]C. Nisoli, Phys. Rev. B **102**, 220401(R) (2020).
[46]Y. Perrin, B. Canals, and N. Rougemaille, Phys. Rev. B **99**, 224434 (2019).
[47]G. Möller and R. Moessner, Phys. Rev. Lett. **96**, 237202 (2006).
[48]C. Nisoli, Eur. Phys. Lett **132**, 47005 (2021).